

## Supplemental Material

# Three-Dimensional Line Edge Roughness in Pre-and Post- Dry Etch Line and Space Patterns of Block Copolymer Lithography

*Shubham Pinge<sup>1</sup>, Yufeng Qiu<sup>1</sup>, Victor Monreal<sup>2</sup>, Durairaj Baskaran<sup>2</sup>, Abhaiguru Ravirajan<sup>1</sup> and Yong Lak Joo<sup>1,\*</sup>*

*1. Robert Frederick Smith School of Chemical and Biomolecular Engineering, Cornell University, Ithaca, NY 14853 (USA)*

*2. EMD Performance Materials Corp., 70 Meister Avenue, Somerville, NJ 08876, USA*

\*E-mail: ylj2@cornell.edu

### **Dry-etching velocities determination**

For a fixed  $V_z$ , we want  $V_x$  and  $V_y$  to be of the similar order and have a narrow spread. Higher  $V_x$  and  $V_y$  will lead to more isotropy in the etching possibly leading to higher roughness. Some of the parameters varied to achieve this narrow velocity spread in  $x$ - $y$  include the energy prefactor,  $\varepsilon$  and  $V_z$ . In figure S1 we can see the effect of varying the energy prefactor on the  $x$ - $y$  component of the velocity. These trials were performed at  $P=10$  mTorr and a fixed  $V_z=0.025$   $\sigma/\tau$ . The Selectivity chosen was substantially high at  $S=75$  approaching an ideal etch. For these trials, lower values of  $\varepsilon$  lead to a narrower velocity spread around zero in the  $x$ - $y$  direction. This would imply higher anisotropy in the etch possible leading to better roughness values. This is also in line with the general behavior of ion-bombardment etch mechanisms which are known to have higher anisotropy compared to reactive-ion etching mechanisms. These trials were repeated for other  $V_z$  and  $P$  in the working regime and the same conclusions were drawn.  $\varepsilon = 0.05$  LJ units were chosen as the default value for subsequent trials.

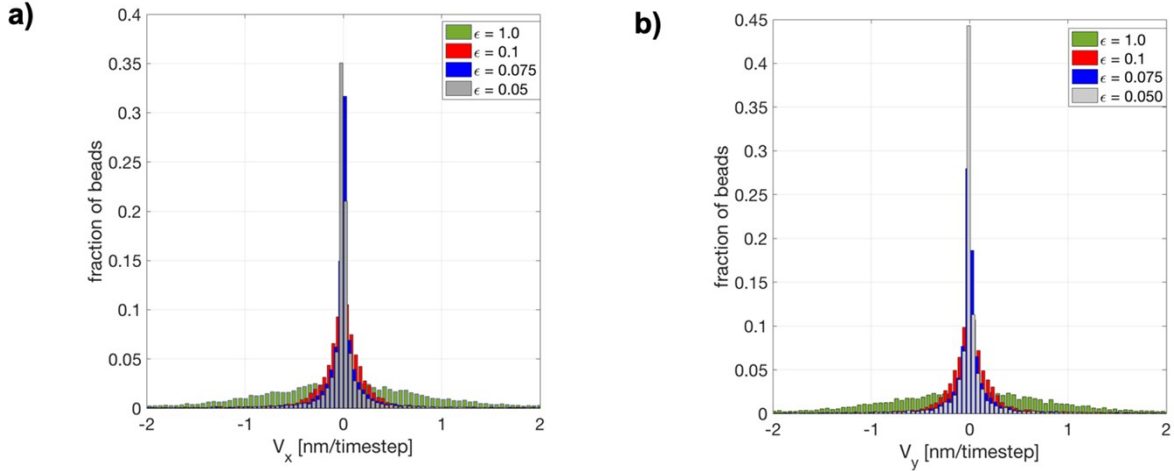


**Figure S1.** Early time velocity distribution for the etch beads for various interaction strengths for the soft-potential. a) x-velocity distribution. b) y-velocity distribution. Z-velocity is constant at  $V_z=0.025 \sigma/\tau$ .

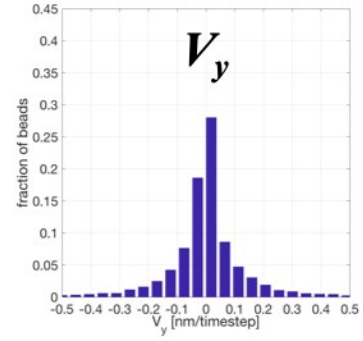
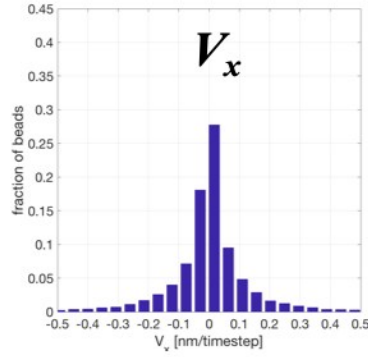
A question that arises from these trials is that what if the interaction between the etch beads were completely turned off by setting  $V_x=V_y=0$  for a fixed  $V_z$ . This would correspond to a system that moves as a focused sheath of particles generated by a plasma source that are completely collisionless. Although, the  $x$ - $y$  velocity spread of these trials were close to a delta function at  $V_x=V_y=0$ , closer inspection of the BCP trajectory showed deficiencies in the assumption. The bead removal for these trials is not appropriate. The etching is uneven through the film thickness which is unphysical. The PS domains also have holes formed leading to porosity issues. The hole formation was more predominant at higher etch pressure. Hence, we can conclude that completely collisionless etch beads are not ideal but weak interactions between etch beads is desired.

Next, we studied the effect of the magnitude of  $V_z$  on the  $x$ - $y$  velocity spread. The following parameters were kept constant:

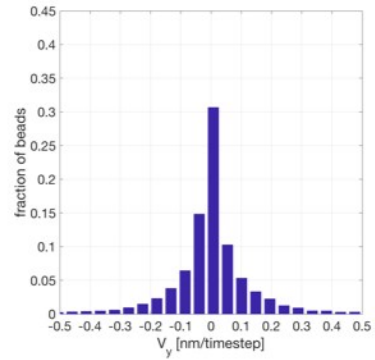
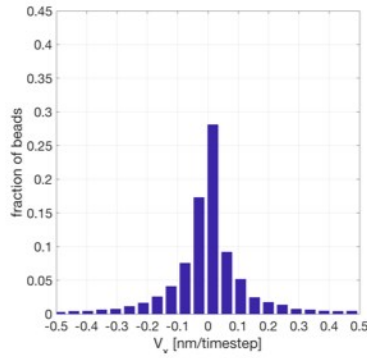
$$\epsilon = 0.05 ; P = 10 \text{ mTorr} ; S = 75 \text{ (ideal etch)} ;$$

As seen in figure S2, higher  $V_z$  leads to a narrower spread in the  $V_x$  and  $V_y$ . This would imply that higher RF power source that results in faster etch beads could possibly lead to lower isotropy in the etch and thus lower roughness.

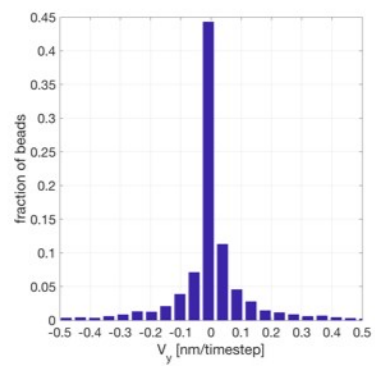
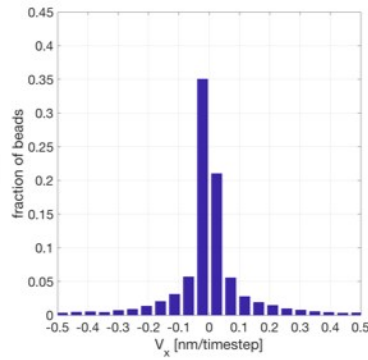
$$V_z = 0.01 \sigma/\tau$$



$$V_z = 0.015 \sigma/\tau$$



$$V_z = 0.025 \sigma/\tau$$



$$V_z = 0.035 \sigma/\tau$$

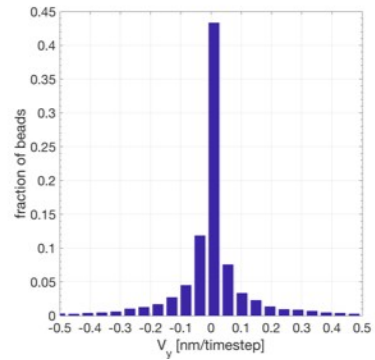
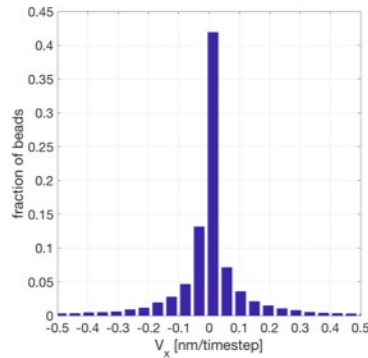


**Figure S2.** Early time x,y-velocity distribution for a constant  $V_z$ . Higher velocity spread leads to narrower distribution.

## Effect of etch gas pressure

For an etch gas with fixed chemistry and at a constant temp, the site density is expressed in terms of gas pressure.

$$\frac{PM}{RT} = \rho \quad (\text{equ. S1})$$

$P$  = pressure in mTorr;  $M$  = molecular weight of the etch gas;  $T$  = temperature in Kelvin. For ambient temperatures, assuming Argon gas chemistry we have,

$$\rho = 0.00214 P \text{ gcm}^{-3} \quad (\text{equ. S2})$$

Scaling with the BCP site density of  $0.85 \text{ beads/nm}^3$ , equivalent to  $1.1 \text{ g/cc}$  we get a etch gas bead density of  $0.00165 P \text{ beads /nm}^3$ . For the current study,  $P = 10, 20, \text{ and } 30 \text{ mTorr}$  have been explored.

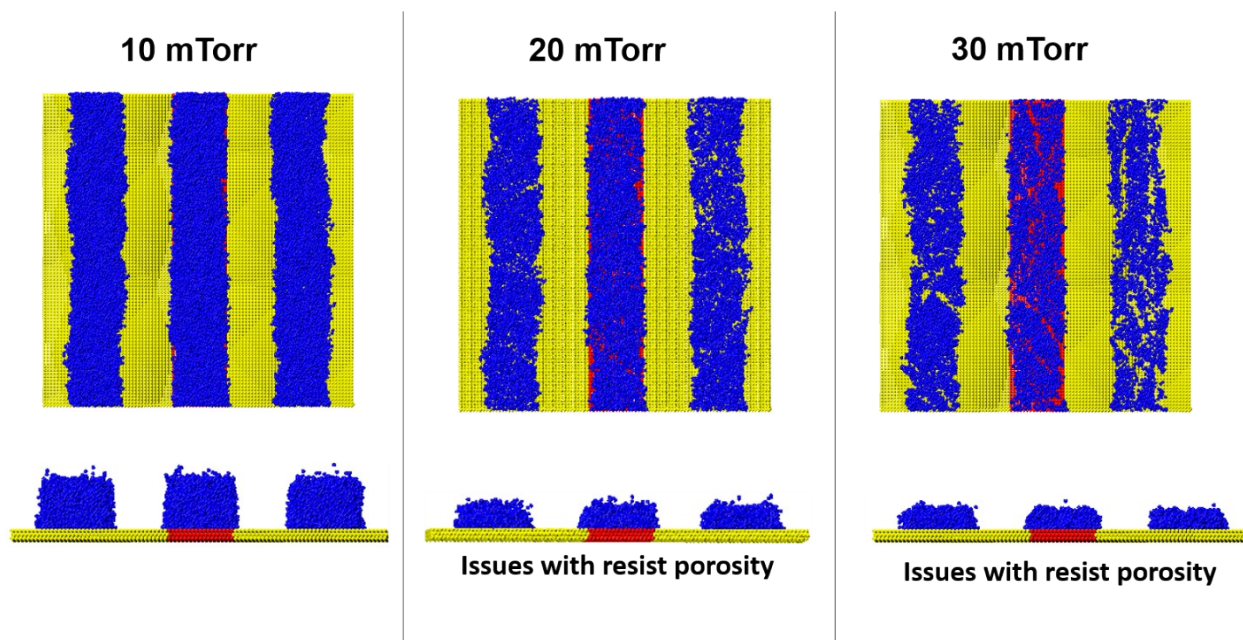


**Figure S3.** Resist morphology at three different etch pressures at a constant  $Vz = 0.0075 \sigma/\tau$  and  $S=3.5$ .

For the optimized  $Vz$  and the soft cosine interaction parameters, the effect of etch gas pressure was studied. For a constant  $Vz = 0.0075 \sigma/\tau$ , default energy prefactor, three system pressures ( $P=10,20, \text{ and } 30 \text{ mTorr}$ ) were studied at the etch selectivity of  $S = 3.5$ . The system morphologies at complete PMMA removal is shown in figure S3. At higher etch gas pressures ( $P = 20 \text{ and } 30 \text{ mTorr}$ ) owing to higher etch bead densities, the resist morphology is more porous than at  $P = 10$

mTorr. A porous etch resist will lead to discrepancies when the pattern is subsequently transferred to the silicon substrate underneath. This issue with resist porosity was also observed for these pressures for  $S = 1.5$  and  $2.5$ . Hence,  $P = 10$  mTorr was chosen as the default pressure for this research.

### **Wet etching**

Although impractical in industry, wet-etching trials were carried out as simulation trials in the research.

After the system is equilibrated below  $T_g$ , in the third process stage, the PMMA phase is selectively etched off under wet-etching conditions. The experimental annealing time is much greater than the etching time-scale ( $\sim 30$  s). We thus simulate the etching process under the following simultaneous conditions: instantaneous breakage of PS-PMMA bonds and removal of PMMA beads followed by addition of etching solvent beads to replace the PMMA beads. The PS domains are thereafter equilibrated along with the etching solvent for the domain morphology to evolve. The etching solvent is ideally poor with respect to PS for high etch selectivity with the solvent quality being governed by the cross-interaction LJ parameter in the WCA potential,  $\epsilon_{\text{PS-solvent}}$ . Figure S4 shows the effect of three solvent types I (blue circle), II (black diamond) and III (red squares) at a reduced temperature of  $T_{\text{etch}} = 0.15, 0.2$  and  $0.25$  on the morphologies of the three PS domains every 2 nm along the film thickness for the flat patterned substrate. Higher the  $\epsilon_{\text{PS-solvent}}$ , poorer is the solvent, better is the quality of etching. Solvent type I and II are poor with respect to PS with  $\epsilon_{\text{PS-solvent-I,rep}} = 0.25$  and  $\epsilon_{\text{PS-solvent-II,rep}} = 0.1$  respectively.  $\epsilon_{\text{solvent-solvent, att}} = 0.2$  for I and II. Solvent type three approaches the behavior of a good solvent with  $\epsilon_{\text{PS-solvent-III,rep}} = 0.05$  and  $\epsilon_{\text{solvent-solvent, att}} = 0.1$ . The pinned domain rests above the PS mat patterning while the other two domains are identified as unpinned-left and right respectively.

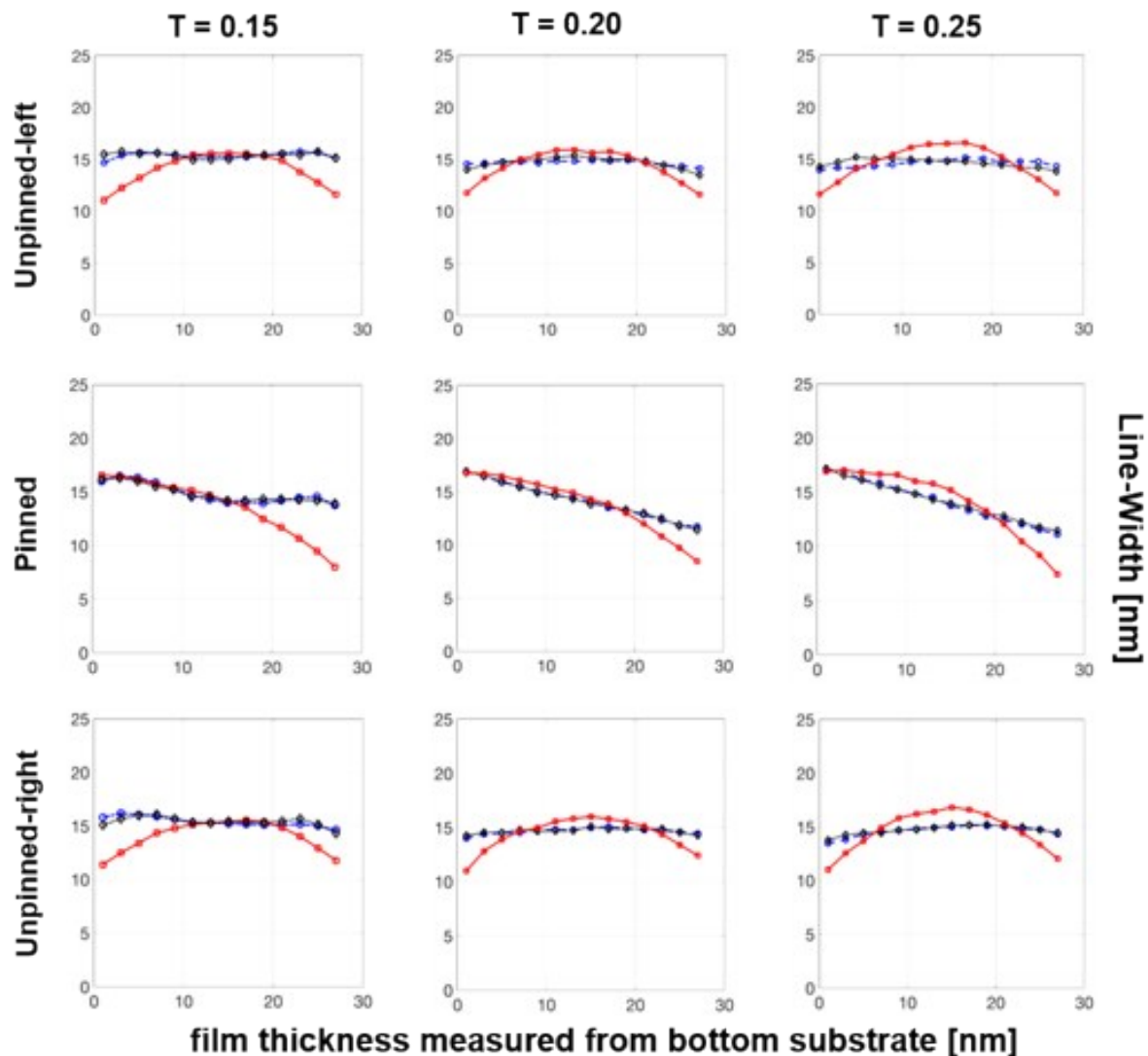


**Figure S4.** PS Line-Width vs film thickness plots for three solvent types. Type I and type II are poor solvents for PS denoted in blue circle and black diamonds respectively. Type III approaches good solvent regime shown in red squares. The PS domain above the PS-mat is pinned.

The results show that etching with solvent III leads to significant pattern collapse for the three temperatures. The pinned domain has a gradient for the Line-Width that tapers away from the bottom substrate. The favorable enthalpic interaction offered by the PS-mat can hold the domain intact close to the bottom substrate but as the interactions fades away from the bottom substrates, the PS-solvent interactions lead to a gradient that spreads at the base and tapers parallel to the film thickness. For the unpinned domains, solvent III bulges close to the middle of the film height caused by the absence of favorable bottom substrate interactions along with the favorable  $\epsilon_{\text{neutral-solvent}}$  interactions. For the poor solvents I and II, the unpinned

domains remain constant in line-width along the film height for the three  $T_{\text{etch}}$ . The pinned domain shows a gradient along the film height for  $T_{\text{etch}} = 0.2, 0.25$ . As the temperature approaches  $T_g$ , PS beads have higher kinetic energy to move and coupled with the favorable PS mat interactions, the line-width tapers away from the substrate.

### LER results

Three phases of LER analysis for the wet-etching on different thickness were executed. As seen in figure S5, the values for averaged LER over the entire film thickness for right and left edges are practically same for the pre- and post-etch stages. The unpinned domains have slightly higher values for the post-etch stage while pinned domains are a little bit higher for the pre-etch stage. The LER averaged values are substantially lower as compared to the annealing values indicating that temperature to be more dominant factor over solvation caused by the poor etching solvent.

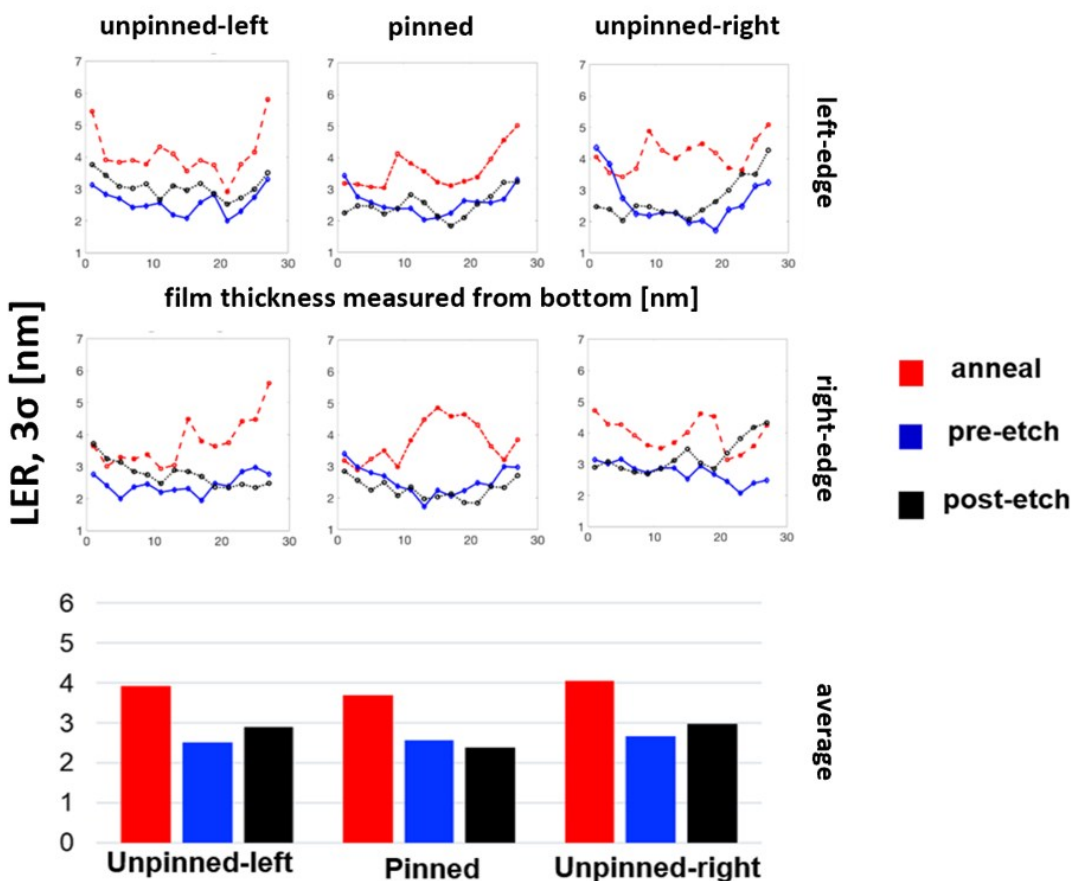


**Figure S5.** LER vs film thickness plots (top 2 rows) and their average values (third row) for the three process stages: anneal (red), pre-etch (blue) and post-etch (black) for flat substrate in a wet-etch system

## PSD results

Power spectral density analysis was carried out on the wet-etching simulation results too. As expected, comparisons between the anneal stage to the cooled stages (pre-and post-etch) shows trend similar to the space domains with the anneal having significantly higher magnitude for the entire spectrum. For lower frequencies, post-etch on average has higher contribution compared to the pre-etch spectrum while for middle (close to correlation frequency) and high frequencies the post-etch spectrum on average is slightly lower than pre-etch. This is especially interesting as the average LER for pre-and post-etch is very close in magnitude in the space domain.

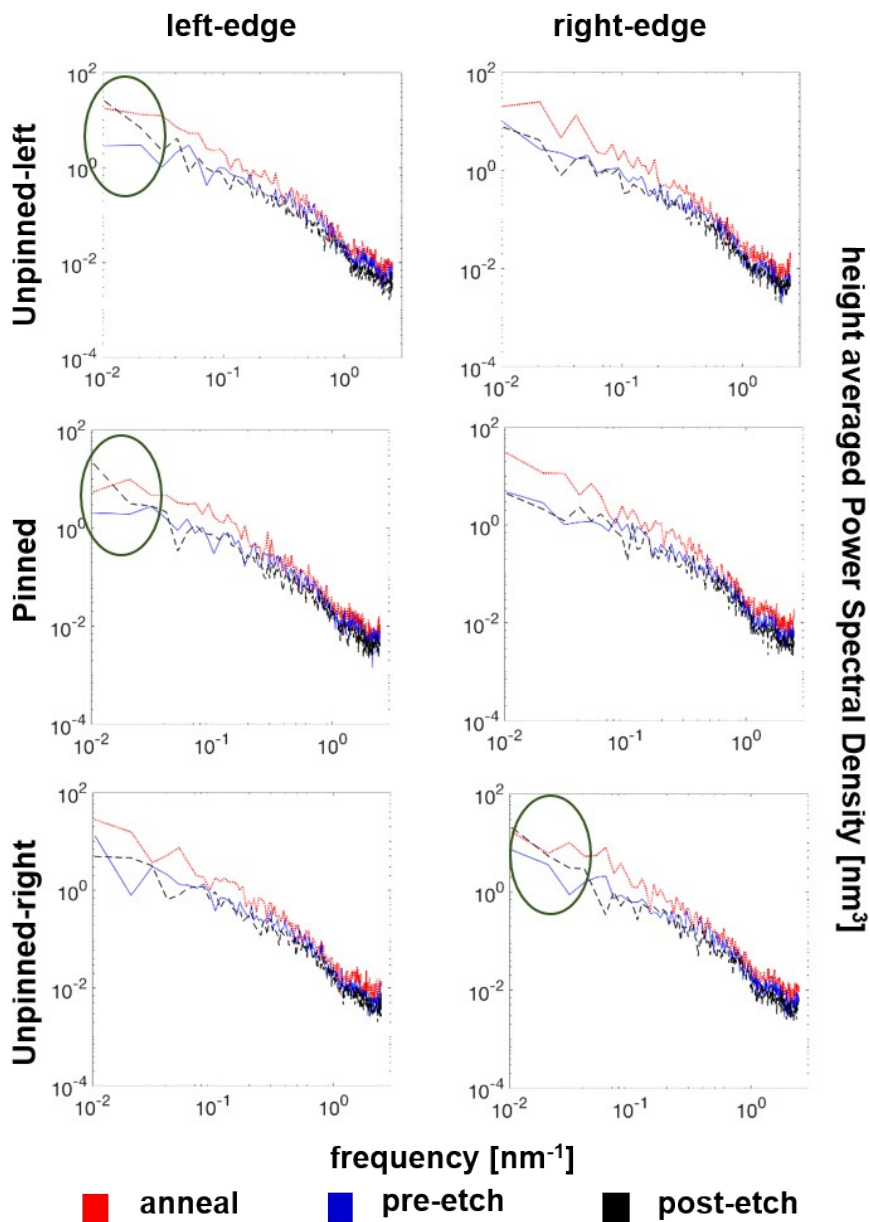


**Figure S6.** Height averaged power spectral density for PS domains for the three process stage for flat substrate geometry.  $\text{PSD}_{\text{anneal}}$  always has the highest contribution. On an average, post-etch has higher lower frequency contribution than pre-etch and reverse in higher frequency range.